Extremely large extinction efficiency and field enhancement in terahertz resonant dipole nanoantennas

Luca Razzari,[1,*] Andrea Toma,[1] Mostafa Shalaby,[2] Matteo Clerici,[2] Remo Proietti Zaccaria,[1] Carlo Liberale,[1] Sergio Marras,[1] Ibraheem A. I. Al-Naib,[2] Gobind Das,[1] Francesco De Angelis,[1] Marco Peccianti,[2] Andrea Falqui,[1] Tsuneyuki Ozaki,[2] Roberto Morandotti,[2] and Enzo Di Fabrizio[1]

[1]*Fondazione Istituto Italiano di Tecnologia, Via Morego 30, 16163 Genova, Italy*
[2]*INRS-EMT, 1650 Boulevard Lionel Boulet, Varennes, Québec J3X 1S2, Canada*
**luca.razzari@iit.it*

Abstract: The distinctive ability of nanometallic structures to manipulate light at the nanoscale has recently promoted their use for a spectacular set of applications in a wide range of areas of research including artificial optical materials, nano-imaging, biosensing, and nonlinear optics. Here we transfer this concept to the terahertz spectral region, demonstrating a metal nanostructure in shape of a dipole nanoantenna, which can efficiently resonate at terahertz frequencies, showing an effective cross section >100 times larger than its geometrical area, and a field enhancement factor of ~280, confined on a lateral section of ~λ/1,000. These results lead to immediate applications in terahertz artificial materials exhibiting giant dichroism, suggest the use of dipole nanoantennas in nanostructure-based terahertz metamaterials, and pave the way for nanoantenna-enhanced terahertz few-molecule spectroscopy and localized terahertz nonlinear optics.

References and links

1. N. Engheta and R. W. Ziolkowski, *Metamaterials: Physics and Engineering Explorations* (Wiley, Hoboken, 2006).
2. V. M. Shalaev, "Optical negative-index metamaterials," Nat. Photonics **1**(1), 41–48 (2007).
3. W. Cai, U. K. Chettiar, A. V. Kildishev, and V. M. Shalaev, "Optical cloaking with metamaterials," Nat. Photonics **1**(4), 224–227 (2007).
4. L. Novotny and N. van Hulst, "Antennas for light," Nat. Photonics **5**(2), 83–90 (2011).
5. J. A. Schuller, E. S. Barnard, W. Cai, Y. C. Jun, J. S. White, and M. L. Brongersma, "Plasmonics for extreme light concentration and manipulation," Nat. Mater. **9**(3), 193–204 (2010).
6. P. Bharadwaj, R. Beams, and L. Novotny, "Nanoscale spectroscopy with optical antennas," Chem. Sci. **2**(1), 136–140 (2011).
7. F. De Angelis, G. Das, P. Candeloro, M. Patrini, M. Galli, A. Bek, M. Lazzarino, I. Maksymov, C. Liberale, L. C. Andreani, and E. Di Fabrizio, "Nanoscale chemical mapping using three-dimensional adiabatic compression of surface plasmon polaritons," Nat. Nanotechnol. **5**(1), 67–72 (2010).
8. S. Kim, J. Jin, Y.-J. Kim, I.-Y. Park, Y. Kim, and S.-W. Kim, "High-harmonic generation by resonant plasmon field enhancement," Nature **453**(7196), 757–760 (2008).
9. S. P. Mickan, A. Menikh, H. Liu, C. A. Mannella, R. MacColl, D. Abbott, J. Munch, and X.-C. Zhang, "Label-free bioaffinity detection using terahertz technology," Phys. Med. Biol. **47**(21), 3789–3795 (2002).
10. B. Ferguson and X.-C. Zhang, "Materials for terahertz science and technology," Nat. Mater. **1**(1), 26–33 (2002).
11. D. Mittleman, *Sensing with Terahertz Radiation* (Springer-Verlag, Berlin, 2003).
12. M. Nagel, P. Haring Bolivar, M. Brucherseifer, H. Kurz, A. Bosserhoff, and R. Büttner, "Integrated THz technology for label-free genetic diagnostics," Appl. Phys. Lett. **80**(1), 154–156 (2002).
13. J. F. Federici, B. Schulkin, F. Huang, D. Gary, R. Barat, F. Oliveira, and D. Zimdars, "THz imaging and sensing for security applications—explosives, weapons and drugs," Semicond. Sci. Technol. **20**(7), S266–S280 (2005).
14. P. Bharadwaj, B. Deutsch, and L. Novotny, "Optical antennas," Adv. Opt. Photonics **1**(3), 438–483 (2009).

15. G. W. Bryant, F. J. García de Abajo, and J. Aizpurua, "Mapping the plasmon resonances of metallic nanoantennas," Nano Lett. **8**(2), 631–636 (2008).
16. P. Mühlschlegel, H.-J. Eisler, O. J. F. Martin, B. Hecht, and D. W. Pohl, "Resonant optical antennas," Science **308**(5728), 1607–1609 (2005).
17. G. Laurent, N. Félidj, J. Aubard, G. Lévi, J. R. Krenn, A. Hohenau, G. Schider, A. Leitner, and F. R. Aussenegg, "Evidence of multipolar excitations in surface enhanced Raman scattering," Phys. Rev. B **71**(4), 045430 (2005).
18. K. B. Crozier, A. Sundaramurthy, G. S. Kino, and C. F. Quate, "Optical antennas: resonators for local field enhancement," J. Appl. Phys. **94**(7), 4632–4642 (2003).
19. F. Neubrech, T. Kolb, R. Lovrincic, G. Fahsold, A. Pucci, J. Aizpurua, T. W. Cornelius, M. E. Toimil-Molares, R. Neumann, and S. Karim, "Resonances of individual metal nanowires in the infrared," Appl. Phys. Lett. **89**(25), 253104 (2006).
20. M. A. Seo, H. R. Park, S. M. Koo, D. J. Park, J. H. Kang, O. K. Suwal, S. S. Choi, P. C. M. Planken, G. S. Park, N. K. Park, Q. H. Park, and D. S. Kim, "Terahertz field enhancement by a metallic nano slit operating beyond the skin-depth limit," Nat. Photonics **3**(3), 152–156 (2009).
21. H. R. Park, Y. M. Park, H. S. Kim, J. S. Kyoung, M. A. Seo, D. J. Park, Y. H. Ahn, K. J. Ahn, and D. S. Kim, "Terahertz nanoresonators: giant field enhancement and ultrabroadband performance," Appl. Phys. Lett. **96**(12), 121106 (2010).
22. M. Seo, J. Kyoung, H. Park, S. Koo, H.-S. Kim, H. Bernien, B. J. Kim, J. H. Choe, Y. H. Ahn, H.-T. Kim, N. Park, Q.-H. Park, K. Ahn, and D. S. Kim, "Active terahertz nanoantennas based on VO2 phase transition," Nano Lett. **10**(6), 2064–2068 (2010).
23. Y. M. Bahk, H. R. Park, K. J. Ahn, H. S. Kim, Y. H. Ahn, D. S. Kim, J. Bravo-Abad, L. Martin-Moreno, and F. J. Garcia-Vidal, "Anomalous band formation in arrays of terahertz nanoresonators," Phys. Rev. Lett. **106**(1), 013902 (2011).
24. F. J. Garcia-Vidal, L. Martin-Moreno, T. W. Ebbesen, and L. Kuipers, "Light passing through subwavelength apertures," Rev. Mod. Phys. **82**(1), 729–787 (2010).
25. F. Blanchard, A. Doi, T. Tanaka, H. Hirori, H. Tanaka, Y. Kadoya, and K. Tanaka, "Real-time terahertz near-field microscope," Opt. Express **19**(9), 8277–8284 (2011).
26. D. J. Shelton, J. W. Cleary, J. C. Ginn, S. L. Wadsworth, R. E. Peale, D. K. Kotter, and G. D. Boreman, "Gangbuster frequency selective surface metamaterials in terahertz band," Electron. Lett. **44**(22), 1288–1289 (2008).
27. A. Berrier, R. Ulbricht, M. Bonn, and J. G. Rivas, "Ultrafast active control of localized surface plasmon resonances in silicon bowtie antennas," Opt. Express **18**(22), 23226–23235 (2010).
28. CST, Computer Simulation Technology, Darmstadt, Germany.
29. R. Adato, A. A. Yanik, J. J. Amsden, D. L. Kaplan, F. G. Omenetto, M. K. Hong, S. Erramilli, and H. Altug, "Ultra-sensitive vibrational spectroscopy of protein monolayers with plasmonic nanoantenna arrays," Proc. Natl. Acad. Sci. U.S.A. **106**(46), 19227–19232 (2009).
30. U. Kreibig and M. Vollmer, *Optical Properties of Metal Clusters* (Springer-Verlag, Berlin, 1995).
31. A. Rice, Y. Jin, X. F. Ma, X.-C. Zhang, D. Bliss, J. Larkin, and M. Alexander, "Terahertz optical rectification from (110) zincblende crystals," Appl. Phys. Lett. **64**(11), 1324–1326 (1994).
32. Q. Wu and X.-C. Zhang, "Free-space electro-optic sampling of terahertz beams," Appl. Phys. Lett. **67**(24), 3523–3525 (1995).
33. C. A. Balanis, *Antenna Theory* (Wiley, Hoboken, 2005).
34. M. Walther, D. G. Cooke, C. Sherstan, M. Hajar, M. R. Freeman, and F. A. Hegmann, "Terahertz conductivity of thin gold films at the metal-insulator percolation transition," Phys. Rev. B **76**(12), 125408 (2007).
35. E. D. Palik, *Handbook of Optical Constants of Solids* (Academic, San Diego, 1998).
36. B. M. Ross and L. P. Lee, "Comparison of near- and far-field measures for plasmon resonance of metallic nanoparticles," Opt. Lett. **34**(7), 896–898 (2009).
37. J. Chen, P. Albella, Z. Pirzadeh, P. Alonso-González, F. Huth, S. Bonetti, V. Bonanni, J. Åkerman, J. Nogués, P. Vavassori, A. Dmitriev, J. Aizpurua, and R. Hillenbrand, "Plasmonic nickel nanoantennas," Small **7**(16), 2341–2347 (2011).
38. N. Liu, M. L. Tang, M. Hentschel, H. Giessen, and A. P. Alivisatos, "Nanoantenna-enhanced gas sensing in a single tailored nanofocus," Nat. Mater. **10**(8), 631–636 (2011).

1. Introduction

Metallic nanostructures have found striking applications both on the macroscale, as building blocks for the so-called metamaterials [1], such as in negative-index materials [2], and optical cloaks [3], as well as on the nanoscale, where nanoantennas [4] and plasmonic nanoconcentrators [5] have become key elements for single-molecule spectroscopy, nano-imaging, and extreme nonlinear optics [6–8]. However, most of these achievements have been so far limited to the visible and infrared regions of the electromagnetic spectrum. On the other hand, terahertz waves, with a frequency ranging from 0.1 to 10 THz, carry the promise of a great impact in fields like label-free detection [9,10], chemical identification [11], medical diagnosis [12], non-destructive imaging and security screening [13]. Indeed, THz radiation (i) can penetrate inside most dielectric materials that may be opaque to visible light, (ii) has low

photon energies that do not cause photoionization in biological tissue, and (iii) exhibits strong dispersion and absorption for numerous molecules. Notwithstanding this, the large wavelength associated with this kind of radiation severely affects the spatial resolution of terahertz spectroscopy, the diffraction limit being roughly half a wavelength (150 μm at 1 THz). In this work, we propose the use of THz resonant nanoantennas to overcome this fundamental limitation and open the route towards the implementation of antenna-enhanced THz spectroscopy at the nanoscale.

An optical antenna can be defined as a device able to convert free-propagating optical radiation to localized energy, and vice versa [14]. The simplest design of an optical antenna is a metallic rod, whose length can be chosen to be half of the effective wavelength [15] of the incoming radiation, realizing a resonant half-wavelength dipole that efficiently captures the incoming free-space wave. When the lateral dimension of the rod is of the order of a few hundred nanometers or less, the electric field localizes into two nanoscale-sized hot spots at the resonator ends, and the device takes the name of "nanoantenna." Resonant nanoantennas have been successfully fabricated and tested in the visible as well as in the infrared frequency range [15–19].

In the terahertz region, nanoslot antennas, which are nanorectangular apertures on a thin layer of gold, have been proposed [20–24]. These structures represent the complementary counterpart of a rod nanoantenna and exhibit very high field enhancement, but present only a 1D localization of the electric field on the plane of the apertures, since they do not confine the radiation along the length of the slot. In addition, the layer of gold, onto which the slots are engraved, compromises the overall transparency of the host medium. Very recently, linear wire [25,26] and bowtie [27] dipole antennas at THz frequencies have been proposed. However, their very large lateral dimension, of the order of tens of microns, have limited the antenna field enhancement factor to 2.6 [25], and the antenna extinction efficiency to ~5 [27]. The half-wavelength THz nanoantennas proposed in this work show instead local field enhancement factors and extinction efficiencies of the order of hundreds.

2. Experimental

An array of aligned planar gold nanoantennas was manufactured by high-resolution electron beam lithography, making use of the following procedure (see Fig. 1(a)): a 120 nm thick PMMA layer was spin-coated on a 500 μm thick, high-resistivity (>10 kΩ·cm), (100)-Si substrate. High-resistivity silicon was selected as a substrate since it is transparent to terahertz

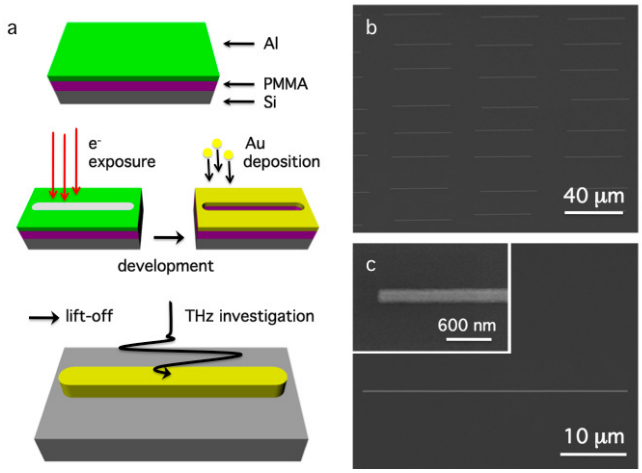

Fig. 1. a, Fabrication details of THz nanoantennas. b, SEM image of the array. The period of the 2D array (20 μm) has been randomized by adding to it a random number with a mean value of 0 μm and a standard deviation of 3 μm. c, SEM high-resolution image of a single nanoantenna (the inset shows a magnification of the nanoantenna end).

radiation, and has a constant refractive index in the region of interest. To prevent charging effects during the electron exposure, a 10 nm thick Al layer was thermally evaporated on the PMMA surface. Electron beam direct-writing of the nanoantenna patterns was carried out using a high resolution Raith150-Two e-beam writer at 20 keV beam energy and 20 pA beam current. After the Al removal in a KOH solution, the exposed resist was developed in a conventional solution of MIBK:IPA (1:3) for 30 s. Then, a 5 nm adhesion layer of Ti and a 60 nm Au film were thermally evaporated in a 10^{-7} mbar vacuum chamber. Finally, the unexposed resist was removed with acetone and rinsed out in IPA.

After extensive electromagnetic simulations performed using a finite-integration-technique based commercial software [28], the nanoantenna length has been chosen to be 40 μm, in order to show a resonance within the bandwidth of the available THz source. The nanoantennas cover a large area of 5x5 mm^2 and their spacing in the two-dimensional array is 20 μm in average in both directions on the plane, and has been randomized (see Fig. 1(b)) to average out the dipolar coupling between neighboring nanoantennas and minimize diffraction effects in the extinction measurements [27,29]. Each nanoantenna is 200 nm wide (thus presenting a very high aspect ratio of 200, see Fig. 1(c)), and 60 nm high.

The fabricated sample was characterized using far field extinction spectroscopy [30]. We employed a standard zinc telluride source [31] producing quasi single-cycle terahertz pulses centered at 1 THz. The terahertz beam was generated by optical rectification in a 500 μm thick, (110)-ZnTe crystal using 800 nm pulses (130 fs time duration, 1.6 mJ energy) delivered by a commercial Ti:sapphire source (Spitfire Pro, Spectra-Physics). A black polyethylene pellicle, transparent to terahertz radiation, was employed to block the remaining 800 nm light transmitted through the ZnTe crystal. The nanoantenna array was illuminated by a collimated terahertz beam with a beam diameter of 7 mm. For detection, we relied on coherent electro-optical sampling [32], focusing the transmitted terahertz pulse on another 500 μm thick (110)-ZnTe crystal. Since terahertz radiation is strongly absorbed by water molecules, all the measurements were carried out in a nitrogen-purged environment.

3. Results and discussion

Figure 2(a) shows the temporal waveforms of the THz pulses transmitted through the sample (normal incidence), for the two cases of polarization parallel (i.e. set along the long axis) and perpendicular (along the short axis) to the nanoantennas. By Fourier transforming these waveforms, the power spectra of the transmitted pulses can be obtained (inset of Fig. 2(a)). When the polarization was set along the short axis of the nanoantennas (blue lines in Fig.

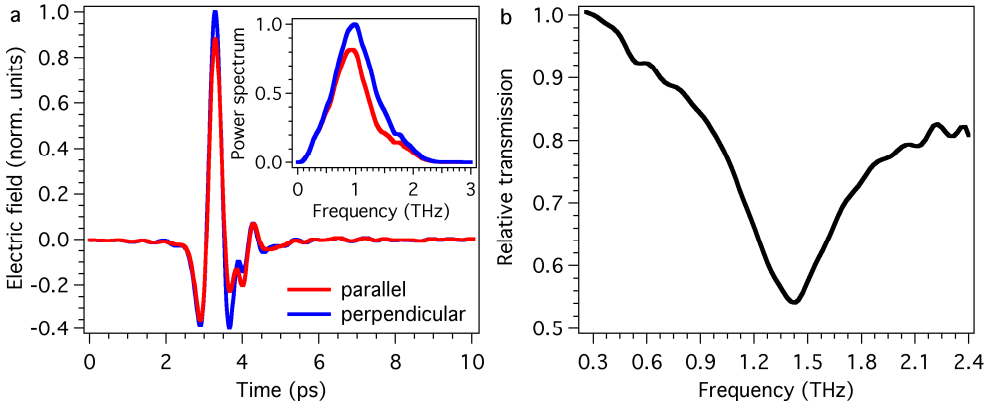

Fig. 2. a, Terahertz temporal waveforms transmitted through the sample, for polarization set parallel (red curve) or perpendicular (blue curve) to the long axis of the nanoantennas. (Inset: correspondent power spectra). b, Relative transmission T_{rel} as a function of frequency, calculated as the ratio of the transmitted spectrum in the case of long axis excitation over the transmitted spectrum for short axis excitation.

2(a)), the transmission of the sample was measured to be substantially identical to that one of a reference silicon substrate with no nanoantennas. This happened because the nanoantennas covering factor (ratio of the area covered by the nanoantennas divided by the overall illuminated area) is only 0.4%. When instead the polarization was set along the long axis of the nanoantennas (red lines in Fig. 2(a)), the transmitted power showed a strong decrease. This is evident from the relative transmittance T_{rel}, calculated as the ratio of the two power spectra of Fig. 2(a), and depicted in Fig. 2(b). A fundamental antenna resonance is revealed, centered around 1.4 THz, in correspondence with a reduction of the transmitted power of ~50%. Incidentally, we want to mention that this transmission change is basically a function of the materials involved and of their shapes. Ideally, a better conductor with sharper edges would exhibit an even stronger transmission reduction [33].

The giant dichroism revealed by Fig. 2(b) can be directly related with the extinction efficiency Q_{ext}, an important physical parameter characterizing the far field properties of a single nanoantenna. In fact Q_{ext}, defined as the ratio of the extinction cross section σ_{ext} of the nanoantenna to its geometric cross section σ_{geo}, can be written as

$$Q_{ext} = \frac{\sigma_{ext}}{\sigma_{geo}} = \frac{A\left(1-T_{rel}\right)}{NLD}, \qquad (1)$$

where A is the illuminated area, and N the number of illuminated nanoantennas, whose length and width are denoted by L and D respectively. Figure 3(a) (open circles) shows the experimentally determined extinction efficiency as a function of frequency. As one can see, Q_{ext} presents a peak with a value of around 110. This means that, under resonance conditions, the dipole nanoantenna increases its effective cross section by 110 times. Such a drastic increase is found to be significantly larger than the one shown by isolated nanoantennas at higher frequencies (Q_{ext} of 20 or lower; see, for example [18], and [19]). On the other hand, at lower frequencies (e.g. in the radio-wave region) the perfect electric conductor approximation holds, and the cross section of a single dipole antenna can be enhanced by a factor even greater than a 1,000 [33].

Numerical simulations were performed, considering nanoantennas with a rectangular lateral section (200x60 nm^2), capped with hemicylindrical ends of radius R = 100 nm, resulting in a total length of 40 μm. The nanoantenna sharp edges are blended with a curvature radius of 20 nm, to more accurately resemble the fabricated structure. The dielectric constant of gold is taken from [34], and the nanoantennas are assumed to be embedded completely in an effective medium with dielectric constant $\varepsilon_{eff} = \left(1+n_s^2\right)/2$, where n_s = 3.42 is the refractive index of the silicon substrate [35]. Periodic boundary conditions are used to simulate the response of an array of nanoantennas, with a spacing of 20 μm in both directions on the plane. The simulations presented hereon were all performed under plane wave illumination at normal incidence, with polarization set along the long axis of the nanoantennas.

Figure 3(b) shows a three dimensional plot of the so-called "radar cross section" [33] of the nanoantenna, close to its resonance. The scattering pattern takes the shape of a flattened torus, as it is the case of a standard half-wavelength dipole antenna for radio waves [33]. The extinction efficiency Q_{ext} can be derived from the simulations, using the calculated total absorption cross section σ_{abs} and total scattering cross section σ_{sca}, through the simple relation: $Q_{ext} = \sigma_{ext}/\sigma_{geo} = \left(\sigma_{abs}+\sigma_{sca}\right)/\sigma_{geo}$. The results of this procedure are plotted in Fig. 3(a) (green curve), for a direct comparison with the experimental data. We note a good agreement between measured and calculated Q_{ext}, both in terms of absolute values and trend. The slight shift that can be observed may be attributed to the uncertainty in the effective dielectric constants of the materials involved, as well as to the effects of the position randomization of the fabricated nanoantennas. The antenna resonance frequency can be even evaluated analytically, under the assumption of perfect electric conductor, through a Fabry-Perot-like

equation estimating the half-wavelength resonance condition: $f = c/\left(2n_{eff}L\right)$, where f is the resonance frequency, c the speed of light in vacuum, and $n_{eff} = \sqrt{\varepsilon_{eff}}$ is the background effective index. This procedure predicts a resonance frequency at 1.49 THz, in fair agreement with both experimental and simulated values.

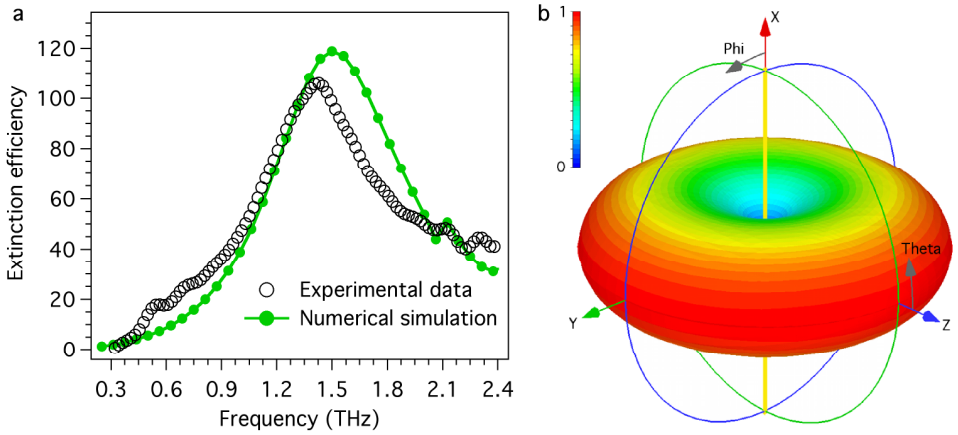

Fig. 3. a, Extinction efficiency Q_{ext} as a function of frequency. Open circles: experimental values obtained using Eq. (1); green curve: numerical simulation. b, Normalized three dimensional representation of the nanoantenna radar cross section, for a frequency of 1.5 THz.

Numerical simulations also give full access to the near field properties of the nanoantenna. Figure 4(a) shows the absolute value of the electric field around the nanoantenna, on a plane that is perpendicular to the direction of the illuminating wave and cuts the nanoantenna exactly at its half height. As expected, the field strongly concentrates at the nanoantenna ends. The full width at half maximum of the field distribution 1 nm away from the nanoantenna end is found to be 180 nm (inset of Fig. 4(b)). This means that the structure successfully concentrate the radiation on a lateral size smaller than λ/1,000. Finally, Fig. 4(b) shows the field enhancement factor F (defined as the ratio of the local electric field to the illuminating

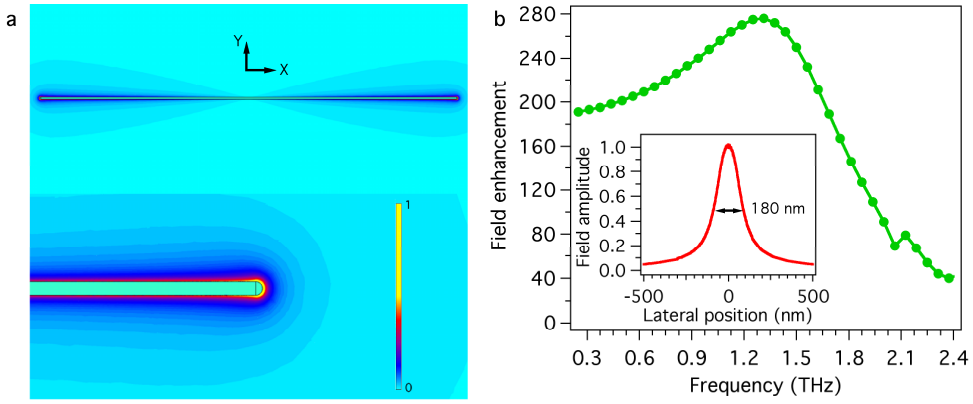

Fig. 4. a, Contour plot of the normalized absolute value of the electric field around the nanoantenna, under resonance conditions (upper part: full view; lower part: magnification of the nanoantenna end). The color ramp has been adapted to allow the visualization of the electric field around all the nanoantenna. b, Field enhancement factor F at the nanoantenna end as a function of frequency. (Inset: normalized electric field profile in proximity of the nanoantenna end. Data are taken 1 nm away from the nanoantenna end in the X direction, and are represented along the Y direction. For X and Y orientation, see a.)

free-space field) at the nanoantenna ends, as a function of frequency. Even in the near field, a broad resonance behavior can be observed, with a peak value of the enhancement of around 280. One can notice that the near field peak broadens toward the low frequency side of the spectrum and is red-shifted, when compared to the far field resonance represented in Fig. 3(a). This kind of behavior has been already observed in nanoantennas at optical frequencies and has been attributed to plasmon damping [36,37]. The high value of the field enhancement reported above holds great promise for applications in THz few-molecule spectroscopy, extending the concept of nanoantenna-enhanced sensing, recently proposed in the visible spectral region [38]. In fact, the effective absorption cross section of a molecule in close proximity of a nanoantenna scales with $|F|^2$ and thus would be enhanced by almost 5 orders of magnitude in our case. In a similar manner, nonlinear interaction at THz frequencies, which are usually very hard to be observed due to the low intensity of the available THz sources, can be strongly enhanced by resonant nanoantennas.

4. Conclusion

We have successfully designed, fabricated and tested dipole nanoantennas that resonate at terahertz frequencies. The far field characterization of these metallic nanostructures has revealed a significant effective dichroism associated with a giant extinction cross section at resonance, more than 100 times larger than the antenna geometric cross section. Besides applications in nanostructure-based terahertz metamaterials, this unique property of terahertz nanoantennas can be used for tomographic labeling of bulk materials such as plastics, fabrics, cardboards, and ceramics, preserving their terahertz transparency when the polarization is set along the short axis of the nanoantennas.

In addition to their significant far field properties, terahertz dipole nanoantennas have shown a field enhancement factor of few hundreds in the near field, opening the route towards the practical implementation of terahertz few-molecule spectroscopy at the nanoscale and of localized terahertz nonlinear experiments.

Acknowledgments

The authors gratefully acknowledge support from European Projects SMD FP7 No. CP-FP 229375-2; Nanoantenna FP7 No. 241818; FOCUS FP7 No. 270483.